

Triple Degree-of-Freedom Piezoelectric Ultrasonic Micromotor via Flexural-Axial Coupled Vibration

Ter Fong Khoo, Dinh Huy Dang, James Friend, *Member, IEEE*, Denny Oetomo, *Member, IEEE*, and Leslie Yeo

Abstract—Actuators remain a limiting factor in robotics, especially in microrobotics where the power density of actuators is a problem. A $3 \times 3 \times 8.7$ mm 3-axis piezoelectric ultrasonic micromotor system is described here in an effort to help solve this problem. Formed from 4 bulk lead zirconate titanate (PZT) thickness-polarized elements placed around the periphery of a rectangular rod, the stator is designed to combine axial and flexural vibrations in a way that permits rotation of a hardened steel ball as a rotor about an arbitrary axis. A simple prototype of the micromotor was found to produce at least a rotation speed of 10.4 rad/s with 4 $\mu\text{N}\cdot\text{m}$ torque about all 3 orthogonal directions at an excitation frequency of about 221 kHz, demonstrating the feasibility of a 3 degree-of-freedom millimeter-scale piezoelectric motor.

I. INTRODUCTION

THIS paper describes the design, analysis, construction, and testing of a $3 \times 3 \times 8.7$ mm triple-axis piezoelectric ultrasonic micromotor system producing triple degree-of-freedom motion by flexural-axial coupled vibrations of 4 thickness-poled piezoelectric elements. The study employed finite element analysis and accurate measurement methods to demonstrate the successful performance of a torsional micromotor capable of producing motion with 3 degrees of freedom.

A common theme in microrobotics research in all its potential applications is the concern with the lack of effective actuators at small scales [1], [2]. Although applications and proposed concepts of actuation in nano-scale technology are being explored, it should be noted that these do not often apply to the tasks in the micro- and millimeter-scale window. Actuation in this range is generally best served through mechanical means. Many important applications lie within this range, for example, critical surgical procedures on various parts of the human body. Eye, brain, middle ear, and gastrointestinal surgical procedures are some of the applications that require very precise motion, dealing with objects in the millimeter to micrometer range, where compact and light micromotors

are essential in delivering precise motion, sufficient torque, and robust performance.

Although there are a variety of methods for performing actuation and certainly innovative research into new materials and methods, a technique that remains promising due to its flexibility, power density, and inherent braking among other features is the use of ultrasonic resonant excitation of flexible structures with piezoelectric materials—so-called ultrasonic motors. Piezoelectric materials have been used for some time to produce actuators [3]–[6]. Further, in contrast to many other technologies, the scaling of both the piezoelectric materials and the actuators that use them to smaller scales is entirely feasible [7]–[11]. Electrostatics, in particular, has long been considered for actuation through the use of silicon microfabrication techniques [12], producing electrostatic micromotors of a few tens of micrometers [13]. However, as motors, these generate very low torque at high speed (on the order of 10 pN·m and 10000 rpm) [14], requiring reduction gears for most practical applications accompanied by the long-known problem of friction and wear [15], especially relevant at these scales.

Beyond the straightforward application of piezoelectric materials to form motors regardless of the size, researchers have used the flexibility inherent in ultrasonic actuation to provide devices capable of rotating objects about 3 orthogonal axes [16]—even for representing the human neck [17]. Although small actuators have been formed to provide this kind of motion [7], the planar configuration is inconvenient for many microbotic applications, as is the high voltage (200 V) required to obtain motion.

In this paper, a piezoelectric micromotor is designed and developed to produce a triple-axis or multi-degree-of-freedom (DOF) micromotor. The paper is organized as follows. The fundamental configuration of the motor is analyzed in the next section, followed by impedance and vibration analysis to identify the location of the resonance modes, finishing with measurement of the performance of a motor prototype. It is finally shown that the resulting micromotor is capable of generating rotation about an arbitrary axis.

II. CONCEPT AND ANALYSIS

In prior work, a single-DOF motor was created by using the in-plane shearing deformation of rectangular lead

Manuscript received April 25, 2008; accepted March 29, 2009. This work was supported in part by an Australian Research Council Discovery Grant DP0773221 and the Monash University Small Grant and New Faculty Grant schemes.

The authors are with the MicroNanophysics Research Laboratory, Department of Mechanical Engineering, Monash University, Clayton, Victoria, Australia (e-mail: james.friend@eng.monash.edu.au).

D. Oetomo is with the Department of Mechanical Engineering, University of Melbourne, Victoria, Australia.

Digital Object Identifier 10.1109/TUFFC.2009.1236

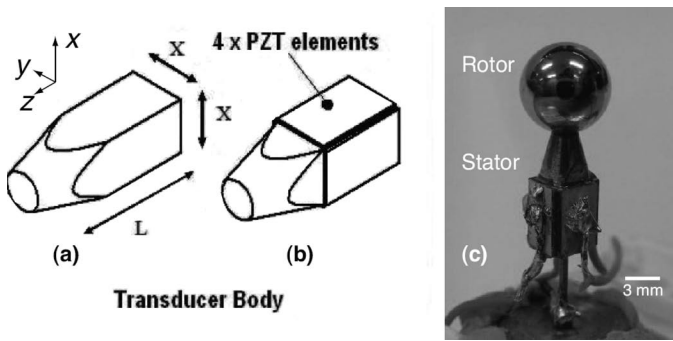


Fig. 1. The (a) square cross section of the stator and (b) placement of the 4 PZT elements eventually leading to a (c) prototype complete with mount, wiring, and rotor.

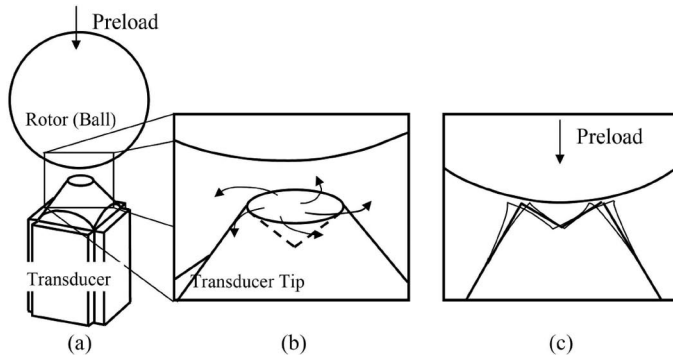


Fig. 2. The overview of the micro motor: flexural motion produced by the appropriate actuation of the 4 PZT elements on the stator yields the rotation of the rotor about an arbitrary axis.

zirconate titanate (PZT, C-203, Fuji Ceramics Co., Ltd., Tokyo, Japan) elements [18]. Replacing those with thickness-polarized PZT elements, it becomes feasible to generate axial and flexural vibrations in a similar structure with the advantages of reduced-loss mounting described in the prior work. Four PZT plates, with the polarization facing outward, are attached on each of the 4 sides of a square cross-sectioned phosphor bronze rod with dimensions defined as (x, x, L) as shown in Fig. 1. The metal stator is grounded, while the outer electrode faces of each piezoelectric element is individually wired to permit separate excitation.

Three DOFs in the rotation of the rotor are obtained through the combination of actuation of the PZT elements. Axial vibration alone is produced by the in-phase actuation of either all 4 PZT elements or 2 on opposing sides of the beam at the axial resonance frequency using a sinusoidal input signal. Flexural vibration about the x -axis, for example, may be obtained by providing a signal to the 2 PZT elements on the y faces of the stator with a 180° out-of-phase signal between them, and flexural vibration about the y axis may be obtained in a similar manner. These signals must be provided at a flexural resonance frequency. If the axial and flexural resonance frequencies are suitably matched, it is then possible to induce elliptical motion at the contact interface (see Fig. 2) about any axis

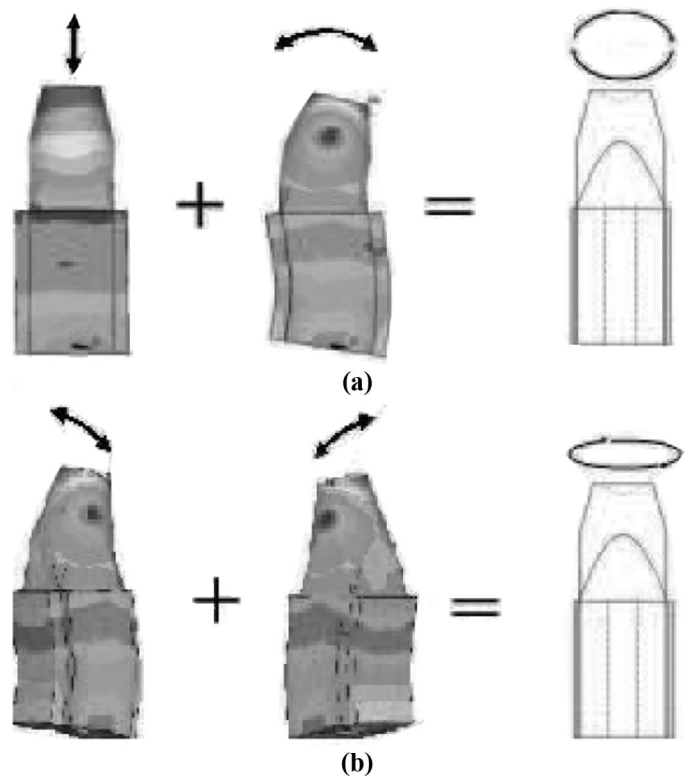


Fig. 3. The superposition of different vibration phenomena with appropriate phase differences between the vibration will deliver rotation of the rotor about (a) either the x or y -axis, using a combination of axial and flexural vibration in a plane perpendicular to the axis of rotation, or the (b) z -axis, using a combination of flexural vibrations in 2 different planes.

using different combinations of the phase and amplitude of these actuation signals, causing rotation of the rotor about an arbitrary axis.

Specifically, rotation about the x and y axes is achieved as shown in Fig. 3(a) by combining the axial and flexural vibrations. A wobble motion, however, is required to obtain rotation about the z -axis as illustrated in Fig. 3(b) with the superposition of 2 perpendicular flexural vibrations. Takemura, *et al.*, showed in their superb paper [16] that if these rotations may be generated in a multi-DOF motor, they may be combined together to provide controlled rotation about any axis.

Adopting a simple approach for determining the axial and flexural resonance frequencies ω_i and ω_j , respectively, the homogeneous constant-cross-sectional area rod axial resonance and Kirchoff flexural resonance frequency equations

$$\omega_i = \frac{(2i - 1)\pi}{2L} \sqrt{\frac{E}{\rho}} \tag{1}$$

and

$$\omega_j = \frac{(\lambda_j L)^2}{L^2} \sqrt{\frac{EI}{\rho A}} \tag{2}$$

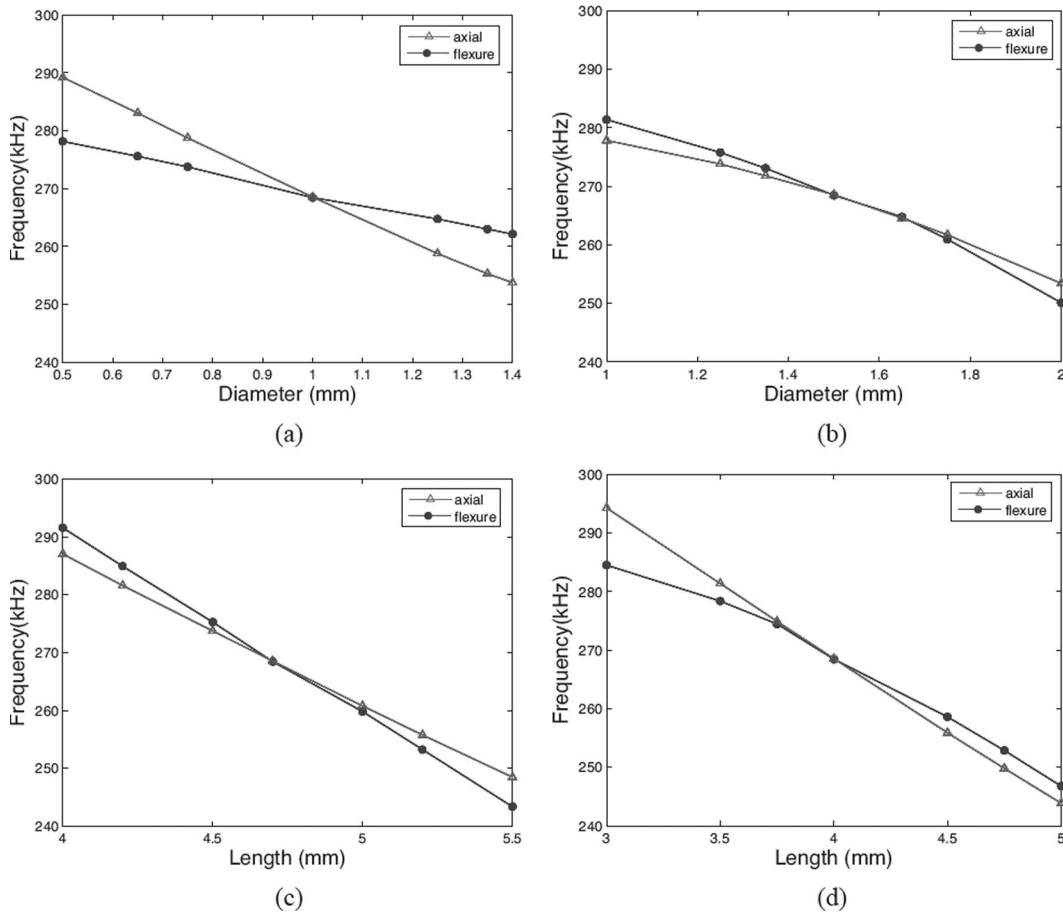


Fig. 4. Remarkably, the (a) horn tip diameter, (b) stress relief hole diameter, (c) body length, and (d) horn length parameters all affect the fundamental axial and flexural resonance frequencies with a sufficient difference to permit selection of a matched axial-flexural resonance frequency. The diameter of the horn and stress relief hole, and the lengths of the body and horn were 1, 1.5, 4.7, and 4 mm, respectively, for the plots shown above, although in the analysis, the trends shown here were similar for a much wider range of the parameters (within a geometrically acceptable range), suggesting the basis is convex.

were used, where λ_j is the wavelength, E is the Young's modulus of motor material, ρ is the density of motor material, I is the second moment of area, A is the cross-section area of the motor body, and L is the length of the motor body.

Equating ω_i and ω_j , the approximate dimensions (x, x, L) , where x is the width and height of the motor, to match these frequencies may be obtained from

$$\frac{L}{x} = \frac{(\lambda_j L)^2}{(2i - 1)\pi\sqrt{3}}. \quad (3)$$

Using this basic equation as a guide, the geometry was modeled in ANSYS (ANSYS, Canonsburg, PA), complete with piezoelectric elements and mounting using modal and harmonic analysis. The results shown in Fig. 4 were obtained by adjusting the parameters, illustrating that with a certain configuration of dimensions, the axial and flexural frequency will converge to the same values. The parameters that could reasonably be changed were the tip diameter of the horn, the diameter of the stress relief hole, the length of the body, and the length of the horn, all relative to a base width $x = 3$ mm chosen for this study.

After the design iteration in ANSYS, the final dimensions of the transducer were selected as shown in Fig. 5. The diameter of the horn and stress relief hole and lengths of the body and horn were chosen to be 1, 1.5, 4.7, and 4 mm, respectively. Phosphor bronze was chosen for the base and horn to keep the resonance frequencies of the system low. A copper stand with a 1-mm-diameter shaft was inserted into a centrally machined hole to serve as a vibration-isolated mount. The tip of the horn was machined with a v-shaped notch to balance and hold the spherical rotor in place.

III. DYNAMIC IDENTIFICATION

To construct the micromotor, 4 PZT elements were bonded to the phosphor bronze transducer using epoxy (see Fig. 5) in a precision electro-discharge machining vise, forming the stator. The vibration modes and resonance frequency measurements were carried out to obtain the dynamic response of the transducer through impedance and laser Doppler vibrometry (LDV). The resonance frequencies of the micro-motor and the associated mode

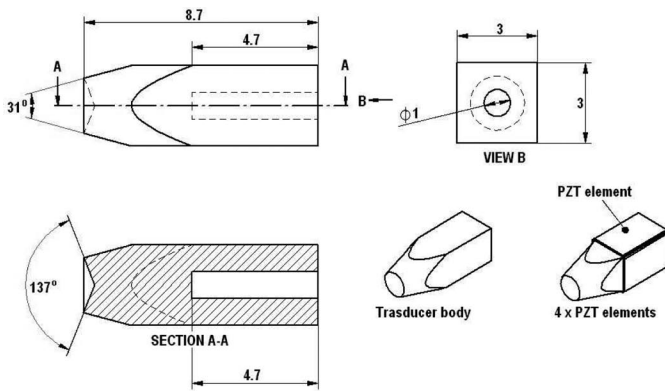


Fig. 5. The final design: $3 \times 3 \times 8.7$ mm with a tapered v-notch in the tip and 4 PZT elements (each with dimensions of $5 \times 3 \times 0.5$ mm thick).

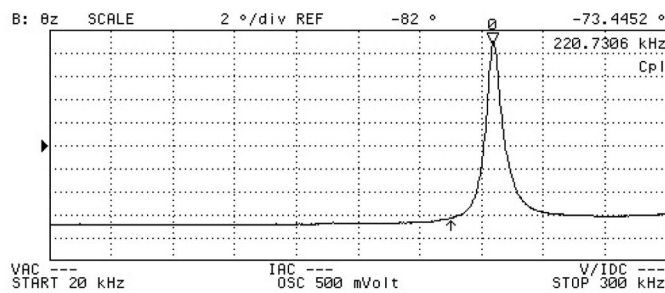


Fig. 6. Impedance spectrum with the connections configured for axial vibration.

shapes were determined through the combined use of an impedance analyzer (4294A, Agilent, Santa Clara CA), and a scanning laser Doppler vibrometer system (MSA-400, Polytec, Waldbrönn, Germany). The impedance analyzer was used to measure the resonance frequency of the transducer while the LDV scans were used to obtain the profile of the transducer vibration modes.

Using the impedance analyzer, the axial resonance frequencies were determined by connecting all piezoelectric elements together on the positive input while connecting the stator to ground—a prominent axial resonance was found at 220.7 kHz, as shown in Fig. 6. Similarly, flexural resonance frequencies were obtained by connecting the pair of PZT elements along either the x -axis or y -axis, one to the positive input and the other to ground, and leaving the other 2 elements and the stator disconnected—with this configuration a prominent flexural resonance frequency was found at 221.3 kHz (Fig. 7).

The LDV was used to determine the axial and flexural vibration modes and frequencies between 100 and 400 kHz. To obtain the profile of the axial vibration, the instantaneous velocity of the tip in the direction of z -axis was measured along the diameter of the tip; see Fig. 8(a) (diameter = 1.8 mm). Fig. 9(a) illustrates the axial vibration mode (instantaneous velocity profile) induced by driving a pair of piezoelectric elements on the $\pm x$ faces of the stator in phase. For flexural vibration, the instantaneous velocity of the stator in the direction of x or y -axis

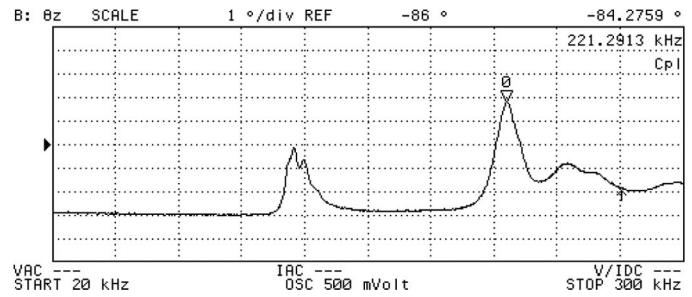


Fig. 7. Impedance analysis with the connections configured for flexural vibration.

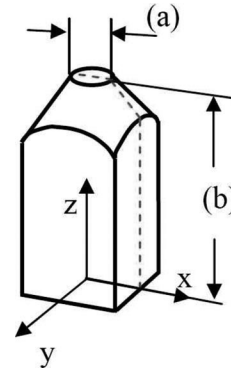


Fig. 8. Laser Doppler vibrometry measurements were performed along (a) the diameter of the tip for axial vibration profile and (b) the length of the stator for flexural vibration profile.

was measured along the length of the stator; see Fig. 8(b) (stator length = 8.5 mm). Fig. 9(b) illustrates the flexural vibration mode induced by driving the same pair of piezoelectric elements on the $\pm x$ faces of the stator 180° out of phase. The remaining 2 piezoelectric elements were grounded. In the latter plot, the vibration amplitude is enhanced by the horn, roughly doubling the vibration velocity from $0.7 \mu\text{m/s}$ at the lower end of the base to $1.2 \mu\text{m/s}$ at the horn tip.

Peaks in the vibration amplitude signals correspond to electromechanical resonance frequencies of the transducers. Axial resonance frequencies were observed at 129.7, 188.1, and 198.5 kHz, and 210.3, 221.4, 268.3, and 397.7 kHz. Flexural resonance frequencies were found at 114.0, 121.0, 215.9, and 219.5 kHz, and 238.3, 264.2, 274.4, and 307.3 kHz. Of these, the strongest peak was observed for a fixed input voltage at a frequency of 221.4 kHz for axial vibration and 219.5 kHz for flexural vibration. These resonances are consistent with the measured electrical resonance frequencies from the impedance in Fig. 7, indicating the electromechanical coupling for these modes is superior to others in the system. It is important to note the rotor is not present for the measurement. Inclusion of the unmodeled rotor mass is known to influence the axial resonance frequency more than the torsional resonance frequency in hybrid torsional transducer devices [19]. However, in our case, no torsional element is involved, and all 4 PZT elements directly actuate the stator in parallel. The effect of the rotor mass could be expected to be equally significant

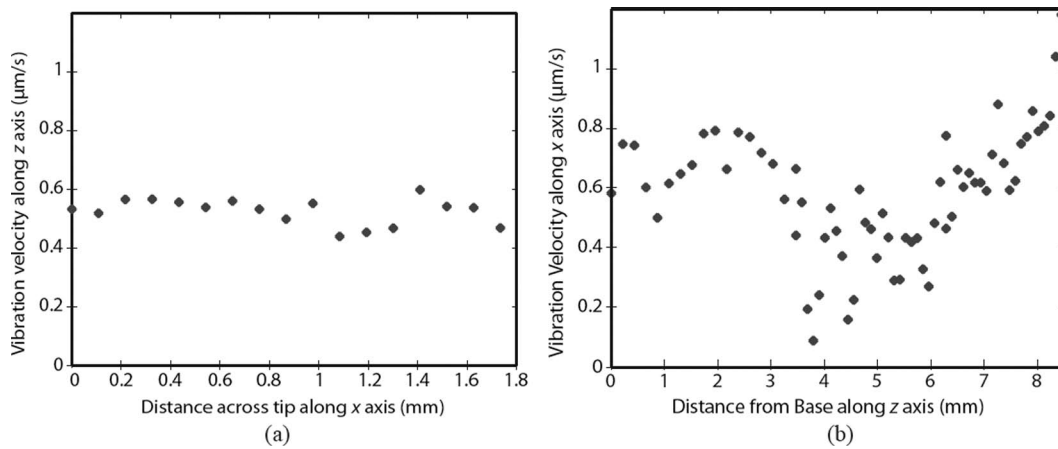


Fig. 9. While exciting axial vibrations, the (a) z -axis-oriented vibration velocity of points across the tip of the stator along the x -axis is fairly constant; see Fig. 8(a). In contrast, while exciting flexural vibrations, the (b) x -axis-oriented vibration velocity of points along the side of the stator down the z -axis is amplified by the horn; see Fig. 8(b).

for both the flexural and axial modes. Furthermore, the system dynamics as contributed by the stiffness of the stator is significantly larger than that by the mass and inertia of the rotor.

In summary, the results of the dynamics identification experiment validate the design analysis as presented in Section II to produce an actuator design with matched axial and flexural frequencies.

IV. MICROMOTOR PERFORMANCE

The actuator's characteristics were measured using the experimental setup shown in Fig. 10. The transducer and its mount were placed vertically on a thin brass plate, and a 11.2-mm-diameter, 6.877-g, hardened steel ball was set on the tip of the transducer. Because the ball is much larger than the tip, the 18° bevel angle of the tip is larger than the 7.8° subtended angle of contact between the ball and tip, and so the ball and tip contacted along a narrow ring around the outer diameter of the tip. By placing the setup on an electronic scale, taring the scale, and then placing the ball on the transducer, the applied preload due to the apparent weight of the ball could be determined.

Through the use of a strong rare-earth magnet as shown in the figure, the weight of the ball on the transducer, and thus the contact preload, could be easily changed [18]. Because the transducer and scale platter were phosphor bronze and aluminum, respectively, the effect of the magnet on the stationary portion of the motor was negligible. However, the attractive force is proportional to the fourth power of the distance between the ball and the magnet, and so care is necessary to accurately manipulate the ball's weight on the transducer tip.

A high speed camera (iSpeed, Olympus, Tokyo, Japan) was used to capture video of the rotation of the ball rotor. Particle tracking software (Diatrack, Semasopt Inc., Chavannes, Switzerland) was then used to track the motion by determining the number of pixels high-contrast points in the image moved between each frame of the video .

The software computes the velocity of tracked objects in the video based on this information, and by rejecting all points in the image frame save for those within a 0.5 mm radius about the center of the ball in the image, parallax effects due to the curvature of the ball were minimized. Over time, the rotation of the ball accelerates to the maximum or no-load speed after applying an input voltage, and once the voltage is removed, the ball slows to a stop—the entire velocity curve was measured at least 3 times. A method developed by Nakamura, *et al.* [20] was used to determine the torque-speed relationship and efficiency of operation from the acceleration of the ball and the coefficient of friction from the deceleration of the ball. The results of the experiments are shown in Figs. 11 to 14.

Fig. 11 illustrates a typical step response of the motor from the image data after postprocessing with the Diatrac software. By applying 2 input voltages to only 2 adjacent piezoelectric elements, 90° out of phase with respect to each other—the $+x$ face and the $+y$ face, for example—and grounding the stator base along with the other 2 sides—the $-x$ face and the $-y$ face—the ball rotor spun about the z -axis due to a superposition of 2 flexural vibrations about the y and x axes, respectively with a 90° phase difference. Inverting the phase difference reverses the direction of rotation. Rotation about the x axis was achieved by applying an in-phase signal to the piezoelectric elements on the $+y$ and $-y$ faces and a second signal to the piezoelectric element on either the $+x$ or $-x$ face; the second signal is 90° out of phase with the first. As before, the remaining, undriven piezoelectric element and the stator base were grounded. In this way, only 2 input signals were necessary to drive the motor, similar to most traveling-wave ultrasonic motors and fewer than required with other multi-DOF motors. It can therefore be summarized that all 3 degrees of freedom in a rotational motion can be achieved by appropriate variations (and phase differences) of actuation signals among the 4 PZT elements.

Changing the input voltage in the voltage-controlled drive of our experimental setup changes the input power with the square of the input voltage and similarly moves

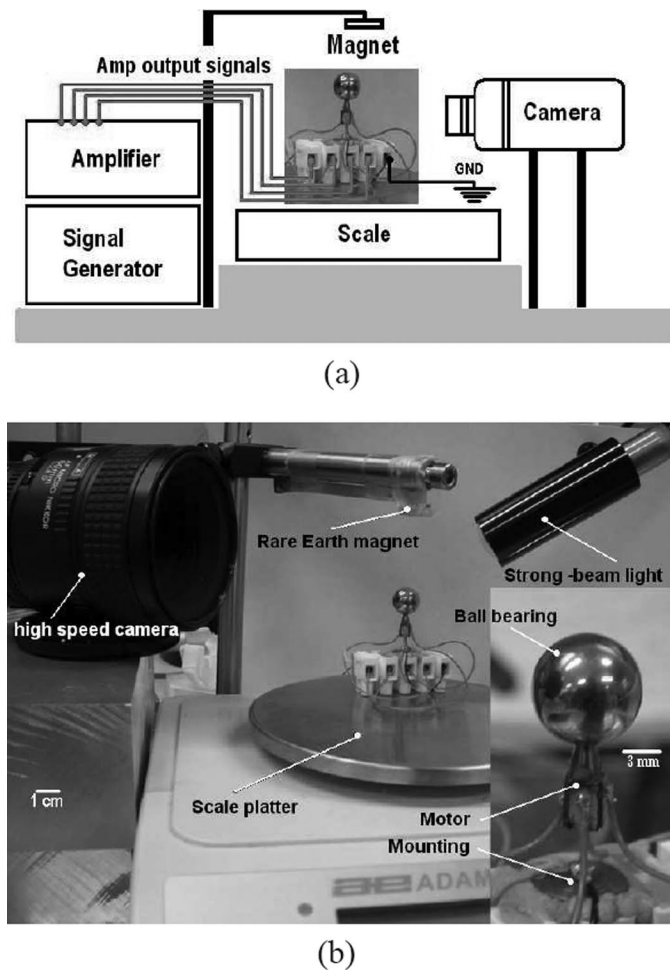


Fig. 10. (a) Schematic and (b) image of the experimental setup for measuring the performance of the motor.

the torque-speed curve toward the upper right as the voltage is increased in Fig. 12 at 67.46 mN preload for the z and y axes—without loss of generality, the latter results also apply to rotation about the x axis. Indeed, the maximum output power of the motor, $1/4 \max \Omega_0 \max T$, generally increases with the square of the applied voltage. However, there is some variability in the maximum torque or speed about either the z axis and the x axis, although the overall output power is not affected. The applied voltages 29.2 and 34.2 V for Fig. 12(a), and the applied voltage of 50 V in Fig. 12(b) are examples; these results were repeatable, and the reason for them would possibly be the different sensitivities of the axial and flexural modes to the input signal. Flexural and axial vibration is generated regardless of the desired rotation axis, and these vibration modes increase at different amplitudes as the voltage is increased on the device. The motion formed at the contact interface varies as a consequence, thereby affecting the maximum torque and maximum speed while not affecting the overall output power. One might expect a nonlinear shift in these values with increasing voltage because axial motion is generated at the contact interface as a consequence of simple flexural vibration through shear in bend-

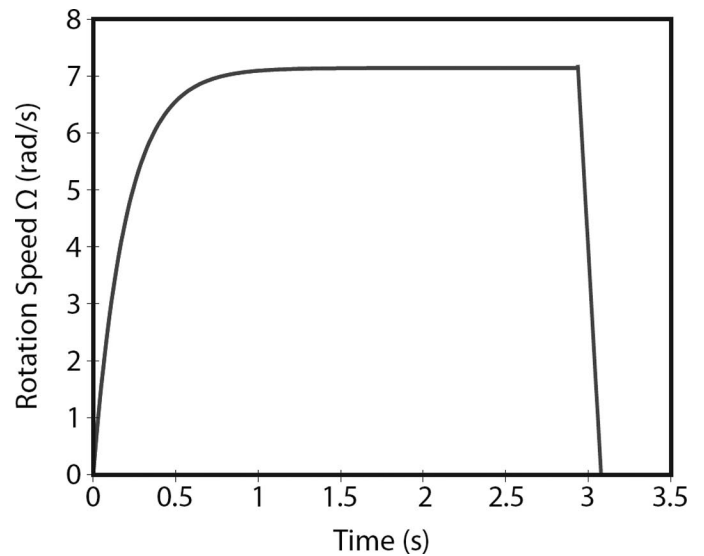


Fig. 11. A typical step response of the motor about the z -axis at 221.0 kHz and at 67.46 mN preload; the rotation behavior about the y - and x -axes are similar.

ing; this form of axial motion appears whether the motor is operated with rotation about the z or y axis.

All torque-speed curves in these plots are linear as a consequence of the model [20], a sometimes controversial result. However, this motor presents rotation behavior almost exactly defined by the exponential acceleration curve espoused by Nakamura, *et al.*, as illustrated in Fig. 11. The use of the model is therefore justified for this particular motor system. With the linear portion of the rotor's deceleration after shutting off the applied signal to the motor, the coefficient of friction was found to be 0.28 ± 0.04 throughout, regardless of the preload or applied voltage.

Fig. 13 shows the rotational speed about the z -axis as a function of the torque for different preloads for input voltages of 29.2 and 45.2 V. The preloads are in the range of 56.68 to 67.46 mN. The maximum no-load speed for each case is 10.41 and 9.14 rad/s, respectively, occurring at the lowest preload for both cases (56.87 and 61.38 mN respectively). As the preload increases, the maximum speed first decreases dramatically to 3.28 and 6.14 rad/s, followed by a gradual increase to 7.14 and 8.48 rad/s, respectively. A similar situation occurs for the torque as it first decreases to a minimum, followed by a gradual increase as the preload is increased. The rapid decrease in rotational speed as the preload is increased from lower to higher values is typical of ultrasonic motors with insufficient preloads due to a transition from period-2 and higher-order, chaotic contact interactions to a purely periodic contact behavior [21] in an extraordinarily complex process. The motor behavior at preloads of 63.74 mN and greater in Fig. 13(a) and 62.26 mN and greater in Fig. 13(b) are representative of a "properly" preloaded motor.

Fig. 14 illustrates the torque-speed curve for rotation about the y axis. The performance about the horizontal axes is inferior to the response about the z axis. As the preload increases, there was a consistent increase in maxi-

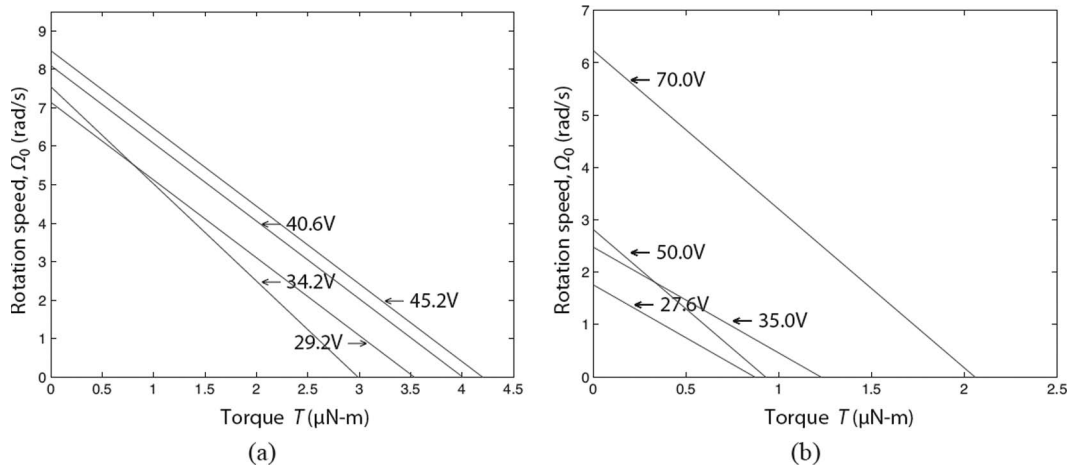


Fig. 12. Motor's rotation characteristics versus applied voltage at 221.0 kHz for the (a) z -axis and (b) y -axis with a 67.46 mN preload.

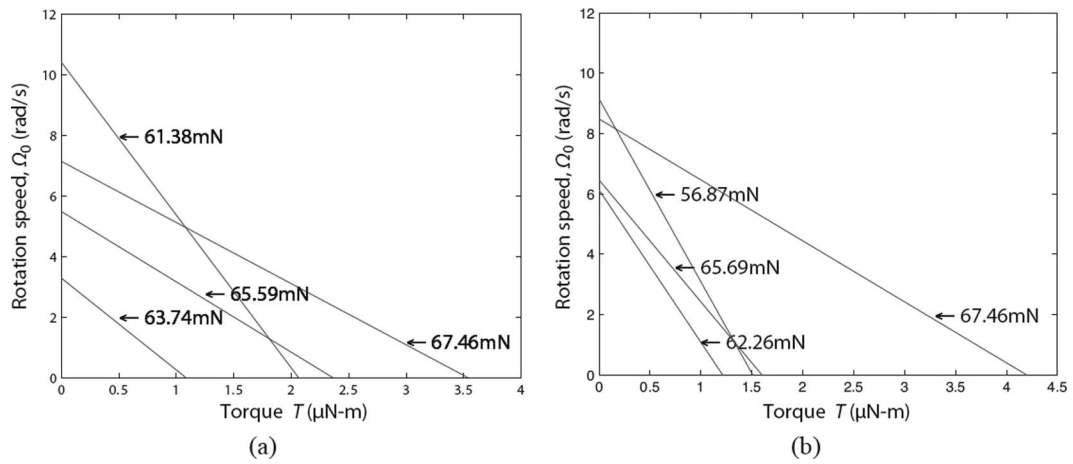


Fig. 13. The rotation characteristics about the z -axis at 221.0 kHz (a) at 29.2 V input and (b) at 45.2 V input under different preload conditions.

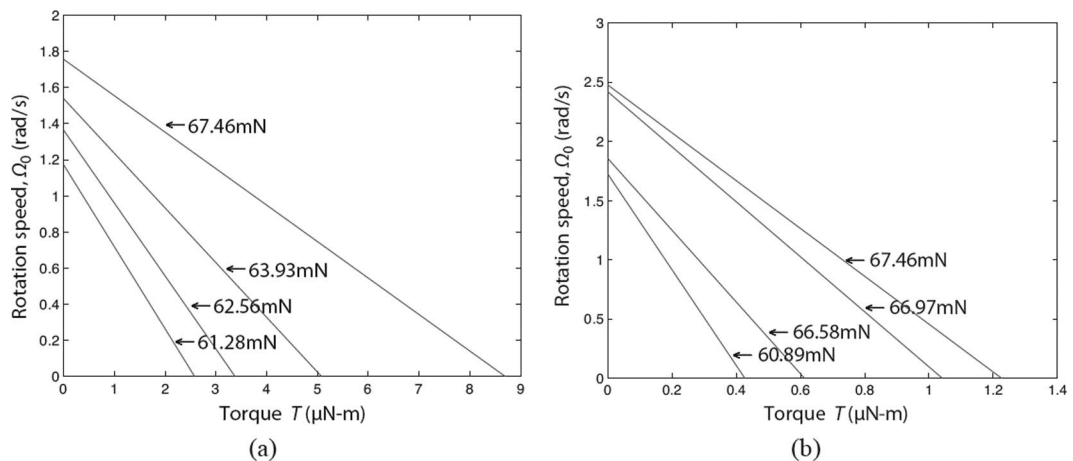


Fig. 14. The rotation performance about the y -axis at 221.0 kHz for (a) 27.2 V input and (b) 35 V input while the preload is varied from 60 to 68 mN.

mum speed and maximum torque. For example, at 27.6 V input voltage and 67.46 mN preload, the maximum no-load speed and torque about the y axis is 1.756 rad/s and 0.87 μNm while it is 2.48 rad/s and 1.22 μNm about the z axis. Curiously, the decreasing rotational speed phenomena at relatively low preloads seen in rotation about the z axis does not appear here. The reason is the preload is already beyond the transition to periodic contact behavior at the interface at the lowest value of preload used in these results. The difference between the transition values of the preload between the 2 cases is caused by the change from a stator vibration displacement ellipse oriented along the plane of contact in z -axis rotation (as a wobble motor) to a vibration ellipse transverse to the plane of contact in y -axis rotation. The rotor's mass is more of a factor in the latter arrangement, because the transverse component of the displacement of the stator is directly imparting an acceleration on the rotor in this case.

V. CONCLUSIONS

A multi-DOF micromotor has successfully been designed and prototyped using bulk PZT materials to drive combined flexural and axial vibrations within a $3.5 \times 3.5 \times 9$ mm square-sided structure with tapered horn, providing at least 2.5 rad/s and 1 μNm at a minimum about each of the 3 axes with operating voltages of 30 to 70 V. Fundamental and bidirectional rotation behavior about the x , y , and z axes that may be superimposed as amply described elsewhere [16] was driven using only 2 input signals switched among the piezoelectric elements. The rotation of the rotor about the x and z axes is provided in the multimedia content online. The 2 signals were used with specific phase differences to obtain elliptical vibration about each axis at the stator tip and therefore rotation behavior about those same axes.

ACKNOWLEDGMENTS

The authors wish to thank the Monash University Engineering Workshop staff.

REFERENCES

- [1] T. Morita, "Miniature piezoelectric motors," *Sens. Actuators A*, vol. 103, no. 3, pp. 291–300, 2003.
- [2] G. Laurent and D. Piat, "Efficiency of swimming microrobots using ionic polymer metal composite actuators," in *Proc. 2001 IEEE Int. Conf. Robotics and Automation*, Washington, DC, 2001, vol. 4, pp. 3914–3919.
- [3] M. Kasuga, A. Iino, K. Suzuki, M. Suzuki, and S. Kotanagi, "Development of self-oscillating ultrasonic micromotor," *J. Jpn. Soc. Precision Eng.*, vol. 32, no. 1, pp. 5–8, 1998.
- [4] A. Flynn, L. S. Tavrow, S. F. Bart, R. A. Brooks, D. J. Ehrlich, K. R. Udayakumar, and L. E. Cross, "Piezoelectric micromotors for microrobots," *J. Microelectromech. Syst.*, vol. 1, no. 1, pp. 14–18, 1992.
- [5] T. Morita, M. K. Kurosawa, and T. Higuchi, "A cylindrical micro ultrasonic motor using PZT thin film deposited by single process

- hydrothermal method," *IEEE Trans. Ultrason. Ferroelectr. Freq. Control*, vol. 45, no. 5, pp. 1178–1187, 1998.
- [6] B. Koc, P. Bouchilloux, and K. Uchino, "Piezoelectric micromotor using a metal-ceramic composite structure," *IEEE Trans. Ultrason. Ferroelectr. Freq. Control*, vol. 47, no. 4, pp. 836–843, 2000.
- [7] M. Aoyagi, S. P. Beeby, and N. M. White, "A novel multi-degree-of-freedom thick-film ultrasonic motor," *IEEE Trans. Ultrason. Ferroelectr. Freq. Control*, vol. 49, no. 2, pp. 151–158, 2002.
- [8] D. Wajchman, D. Liu, J. Friend, and L. Yeo, "An ultrasonic piezoelectric motor utilizing a non-circular cross sectioned twisted beam," *IEEE Trans. Ultrason. Ferroelectr. Freq. Control*, vol. 55, no. 4, pp. 832–840, 2008.
- [9] J. Friend, L. Yeo, and M. Hogg, "Piezoelectric ultrasonic bidirectional linear actuator for micropositioning fulfilling Feynman's criteria," *Appl. Phys. Lett.*, vol. 92, art. no. 014107, 2008.
- [10] J. Friend, Y. Gouda, K. Nakamura, and S. Ueha, "A 5-mm3 bidirectional precision linear microactuator—the Baltan actuator," *IEEE Trans. Ultrason. Ferroelectr. Freq. Control*, vol. 53, no. 6, pp. 1160–1168, Jun. 2006.
- [11] B. Watson, J. Friend, and L. Yeo, "Piezoelectric ultrasonic resonant motor with stator diameter less than 250 microns: The Proteus motor," *J. Micromach. Microeng.*, vol. 19, art. no. 022001, 2009.
- [12] Y. C. Tai and R. S. Muller, "IC-processed electrostatic synchronous micromotors," *Sens. Actuators A*, vol. 20, no. 1, pp. 49–55, 1989.
- [13] W. Trimmer, "Design considerations for a practical electrostatic micromotor," *Sens. Actuators A*, vol. 11, no. 2, pp. 189–206, 1987.
- [14] M. Mehragany and Y. C. Tai, "Surface micromachined mechanisms and micromotors," *J. Micromech. Microeng.*, vol. 1, no. 1, pp. 73–85, 1991.
- [15] S. L. Miller, J. J. Sniegowski, G. LaVigne, and P. J. McWhorter, "Friction in surface-micromachined microengines," in *Proc. SPIE*, vol. 2722, p. 197, 1996.
- [16] K. Takemura and T. Maeno, "Design and control of an ultrasonic motor capable of generating multi-DOF motion," *IEEE/ASME Trans. Mechatron.*, vol. 6, no. 4, pp. 499–506, 2001.
- [17] C. H. Yun, S. Niwano, J. Friend, K. Nakamura, and S. Ueha, "Support mechanism for the ball rotor in the three-degree-of-freedom ultrasonic motor," *Jpn. J. Appl. Phys.*, vol. 42, pt. 1, no. 5B, pp. 3000–3001, 2003.
- [18] J. Friend, K. Nakamura, and S. Ueha, "A piezoelectric micromotor using in-plane shearing of PZT elements," *IEEE/ASME Trans. Mechatron.*, vol. 9, no. 3, pp. 467–473, 2004.
- [19] K. Nakamura, M. Kurosawa, and S. Ueha, "Characteristics of a hybrid transducer-type ultrasonic motor," *IEEE Trans. Ultrason. Ferroelectr. Freq. Control*, vol. 38, no. 3, pp. 188–193, 1991.
- [20] K. Nakamura, M. K. Kurosawa, and S. Ueha, "An estimation of load characteristic of an ultrasonic motor by measuring transient responses," *IEEE Trans. Ultrason. Ferroelectr. Freq. Control*, vol. 38, no. 5, pp. 481–485, Sep. 1991.
- [21] K. C. Liu, J. Friend, and L. Yeo, "The behavior of bouncing disks and pizza tossing," *EPL*, vol. 85, art. no. 60002, 2009.



Ter Fong Khoo received his B. Eng (Mechatronics) degree in 2007 from Monash University, Clayton, Victoria, Australia. Currently, he is involved in the railway signaling industry designing level crossings.



Dinh Huy Dang, a mechatronics engineer, achieved his B.E. degree at Monash University, Clayton, Victoria, Australia, in December 2007. He is interested in both robotics and nano/micro technology. Currently, he is working as a new product integrator (NPI) for Intel Corporation in the CPU and chipset assembly/testing/manufacturing (ATM) sector.



James Friend received the B.S. degree in aerospace engineering, and the M.S. and Ph.D. degrees in mechanical engineering from the University of Missouri-Rolla in 1992, 1994, and 1998, respectively. He received two awards—the AIAA Jefferson Student Goblet and ASME Presentation Award—for his presentation on ultrasonic motor analysis at the AIAA/ASME/AHS/ASC 26th Annual Structural Dynamics Conference in 1996, an award for the encouragement of young scientists at the Symposium for Ultrasonic Electronics and

Engineering in 2003 for a presentation on acoustic waveguides, an award in 2004 for a presentation on the Scream actuator at the Spring Meeting of the Acoustical Society of Japan, excellence in teaching and early career researcher awards from the Monash Faculty of Engineering in 2007 and 2008, respectively, and a Future Leader Award from the Davos Future Summit in Sydney in 2008.

Dr. Friend joined Monash University in Clayton, Victoria, Australia, in late 2004, and founded and co-directs the \$6.5 million MicroNanophysics Research Laboratory with clean room and biolab and a current staff of 3 academics, 3 postdoctorates, and 13 Ph.D. students. He is an associate professor and deputy head of the Department of Mechanical and Aerospace Engineering at Monash University, with research interests in micro/nanodevices for biomedical applications. He is a member of IEEE, ASME, Golden Key, the Lifeboat Foundation for the safe uses of nanotechnology, and a committee member of IEEE Nanotechnology for Biology, and has more than 100 peer-reviewed publications, with 5 book chapters, 49 peer-reviewed journal papers, and 13 patents and patent applications.



Denny Oetomo completed his B.Eng (Honours 1st class) degree in 1997 from the Australian National University and his Ph.D. degree in mechanical engineering from the National University of Singapore in 2004. From 1998 to 1999, he worked as a photolithography engineer for Hewlett-Packard Singapore. From 2002 to 2004, he was a research engineer at the Singapore Institute of Manufacturing Technology. He was a postdoctoral fellow at Monash University, Clayton, Victoria, Australia, and at INRIA Sophia-Antipolis, France,

from 2004 to 2007. He joined the University of Melbourne as a lecturer in January 2008. He has worked in the research areas of robotics, specifically in the kinematic and dynamic analysis of manipulators, mobile manipulation, unified force/motion control, and computational kinematics. He is also involved in the application of robotics in biomechanics.



Leslie Yeo is currently an Australian research fellow and senior lecturer in the Department of Mechanical & Aerospace Engineering and co-director of the Micro/Nanophysics Research Laboratory at Monash University, Clayton, Victoria, Australia. He received his Ph.D. degree from Imperial College, London, UK, in 2002, for which he was awarded the Dudley Newitt prize for a computational/theoretical thesis of outstanding merit. Prior to joining Monash University, he was a

mathematical modeller at Det Norske Veritas UK and a postdoctoral research associate in the Department of Chemical & Biomolecular Engineering at the University of Notre Dame, Notre Dame, IN. Dr Yeo was the recipient of the 2007 Young Tall Poppy Science Award from the Australian Institute for Policy & Science “in recognition of the achievements of outstanding young researchers in the sciences including physical, biomedical, applied sciences, engineering and technology,” and a finalist in the 2008 Eureka Prize People’s Choice Award. His work on microfluidics has been featured widely in the media, for example, on the Australian Broadcasting Corporation’s science television program Catalyst, 3RRR radio broadcast, and in various articles in *The Economist*, *The Washington Times*, *The Age*, *ABC Science Online*, and *Discovery Channel Online*. Dr Yeo is the author of more than 70 research publications, and he holds more than 10 patent applications. He is currently the associate editor of the American Institute of Physics journal *Biomicrofluidics*.